RSC Advances

Journal Name

ARTICLE

Detection of Terahertz Radiation from 2.52 THz CO_2 Laser Using 320 × 240 Vanadium Oxide Microbolometer Focal Plane Array

Received 00th January 20xx,
Accepted 00th January 20xx

DOI: 10.1039/x0xx00000x

www.rsc.org/

Jun Gou[a]†, Jun Wang[a], Xing Zheng[a], Deen Gu[a], He Yu[a] and Yadong Jiang[a]

Real-time, continuous-wave terahertz (THz) detection and imaging are demonstrated with a 2.52 THz far – infrared CO_2 laser and a 320 × 240 vanadium oxide (VO_x) micro-bolometer focal plane array. Nanostructured titanium (Ti) thin film absorber is integrated in the micro-bridge structure of VO_x micro – bolometer by a combined process of magnetr sputtering and reactive ion etching (RIE), and its improvement of THz absorption is verified by optical characteristics test. By eliminating background signal, non uniformity and noise with proper circuits, the output dynamic range of the readout integrated circuit (ROIC) is 0.4V ~ 3.6V and the fixed pattern noise (FPN) is less than 10 mV. After vacuum packaging, the detector is used for THz detection and achieves a responsivity of 2186 V/W and a NEP of 45.7 pW/$Hz^{1/2}$. With this detecting system, THz imaging through wiping cloth and envelope is demonstrated, showing the feasibility of real-time security checking and mail screening.

Introduction

Terahertz (THz) radiation, 0.3 – 10 THz (1 mm to 30 μm), has several properties that make it attractive for imaging applications in security [1–2] and medical [3–4] fields: higher image resolution compared to microwaves with longer wavelength and better penetration of materials compared to infrared radiation with shorter wavelength [5]. For these applications, real – time THz imager is highly desirable. Since uncooled infrared (IR) micro – bolometer focal plane array has been developed for more than 20 years and a series of products are supplied by companies including Raytheon [6–7], BAE [8] and DRS [9], it is an effective method to realize room temperature THz imaging by applying IR detection technology to THz band [10-13], based on temperature and resistance changes of sensing element which are proportional to the absorbed THz energy. However, due to poor absorption of THz radiation, conventional uncooled IR microbolometers with a noise equivalent power (*NEP*) of about 14 pW [14] in the IR range generally have a *NEP* of approximately 300 pW [10, 15] for the THz range, which causes low sensitivity. So it is necessary to design a pixel membrane structure to efficiently absorb THz radiation without compromising the thermal proprieties of the sensors. Nanometer – scale metallic films with low thermal capacity and high thermal conductivity, such as Gold (Au) [16], Nickel (Ni), Chromium (Cr) [17], Nickel – Chromium (NiCr) [18-19], are known to provide good THz absorption due to resistive loss in the film [20]. However, it is not easy to integrate these materials in microbolometers for they can hardly be patterned by dry etching process which is compatible with the fabrication process of microbolometers. Compared to these metallic films titanium (Ti) thin film, can be easily prepared by sputtering and patterned by reactive ion etching (RIE), provides good processing compatibility when used as a THz absorption layer.

This paper presents experimental results on real – time detection and imaging of 2.52 THz radiation from far – infrared CO_2 laser, using 320 × 240 vanadium oxide (VO_x) microbolometer focal plane array with a nanostructured Ti thin film absorber prepared by a combined process of magnetron sputtering and reactive ion etching (RIE). Firstly, nanostructured Ti films are prepared with different thicknesses and the improvement of THz absorption is analyzed by surface morphology test. Then, micro-bridge fabrication is described and optical characteristics is tested. Readout circuit for eliminating background signal, non uniformity and noise is designed, vacuum assembly structure and packaging process are also described. Finally, responsivity and *NEP* of pixel are evaluated and THz imaging through wiping cloth and envelope is demonstrated.

Preparation and Characterization of Nanostructured Ti Thin Film

A sputtering equipment (Varian 3280) was used to prepare Ti thin films by magnetron sputtering of a high purity Ti target in an Ar atmosphere. Ti films were deposited on p – type silicon (100) wafers with a thickness of 20 nm, which was the minimum thickness that could be directly prepared by Varian 3280 limited by its high sputtering rate. In order to obtain nano – scale Ti film with a smaller thickness, RIE was used to

[a] State Key Laboratory of Electronic Thin Films and Integrated Devices, University of Electronic Science and Technology of China, No. 4, Section 2, North Jianshe Road, Chengdu 610054, People's Republic of China
† Corresponding author. Tel.: +86 2883207086; Fax: +86 2883206123; E-mail addresses: goujun@uestc.edu.cn

thin the films with the same process parameters and different etch time. As shown in Tab. 1, Ti thin films with 5 different thicknesses from 5 nm to 16 nm were prepared, respectively. The thinning processes were carried out by a RIE system (P 5000) using a gas mixture of BCl_3 and Cl_2 with a RF power of 50 W, a pressure of 18 mtorr, a BCl_3 flow of 50 sccm, an Cl_2 flow of 10 sccm, and a chamber temperature of 85 ℃. The etching process provided a low Ti etch rate of 6 nm/min and a low etching non uniformity of ≤ 3 % ($NU\%=(E_{max}\text{-}E_{min})/2E_{ave}\times100\%$, where E_{ave} was the average etch rate at 9 test points on the wafer, $E_{max}\text{-}E_{min}$ was the range of etch rate on the wafer), which was suitable for better control of film thickness and uniformity. Film thickness after etching was monitored by square resistance test using a four probe tester (D41-11C/ZM) and calculated through the relationship between square resistance and thickness. Transmissions and reflection of the films were measured by a Fourier transform infrared spectroscopy (FTIR) system (PerkinElmer Spectrum 400).

Table 1 Parameters of Ti thin films prepared by a combination of magnetron sputtering and RIE

	Etch time(s)	square resistance(Ω/□)	Thickness(nm)
1	450	160	5
2	330	88.9	9
3	240	69.6	11.5
4	180	57.1	14
5	120	49.9	16

The measured transmission and reflection curves of Ti thin films thinned by RIE with different thicknesses are shown in Fig. 1 (a) and Fig. 1 (b), respectively. Here, it is not accurate to calculate the absorption of Ti thin film at the same frequency for different light paths for transmission and reflection tests. But we can do qualitative comparison of reflection and transmission to discuss absorption performance of Ti films. It can be seen from Fig. 1 (a) that THz transmission of Ti thin film decreases with the increase of film thickness. Fig. 1 (b) shows that THz reflection of Ti thin film decreases with the increased thickness when the thickness is larger than 9 nm. But the reflection of Ti thin film with a thickness of 9 nm is lower than that of Ti thin film with a thicknesses of 5 nm. It seems that 9 nm Ti film has a lower transmission and reflection compared to 5 nm Ti film, which implies its higher absorption of terahertz radiation due to the relationship between transmission (T), reflection (R) and absorption (A): $T + R + A = 1$. The optimized thickness is similar to that of NiCr thin film prepared by similar method in our earlier research [21] for Ti thin film has a similar value of electrical conductivity with NiCr thin film.

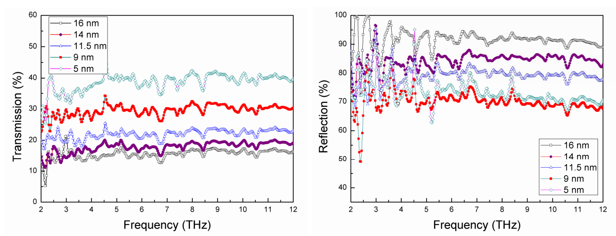

(a) (b)

Fig. 1 The measured (a) transmission and (b) reflection curves of Ti thin films thinned by RIE with different thicknesses

In order to study surface morphology and structure of Ti thin film, Fig. 2 shows the AFM images of 20 nm Ti thin film directly deposited by magnetron sputtering and 9 nm Ti thin film prepared by a combination of magnetron sputtering and RIE. It is clear that the directly deposited Ti thin film has a very smooth surface while the RIE treated Ti thin film has a roughened surface. Nanostructured Ti thin film is obtained by RIE with nano – scale surface structures and a increased specific surface area. It is known that the absorption of a metal film consists of two components [19, 22]: the intrinsic absorption of an ideally smooth surface and the contribution due to nano – scale surface structures, which contributed to the enhancement of THz absorption. So the combined process of magnetron sputtering and RIE can prepare Ti thin film with a small thickness by precise control of RIE process, at the same time it is an effective method to obtain nanostructured Ti thin film for further improvement of THz absorption.

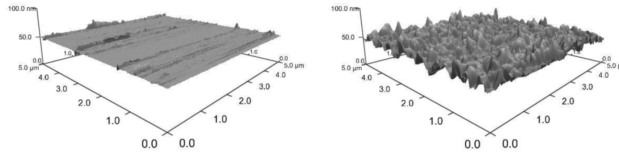

(a) (b)

Fig. 2 SEM images of (a) 20 nm Ti thin film directly deposited by magnetron sputtering and (b) 9 nm Ti thin film prepared by a combination of magnetron sputtering and RIE

Micro – bridge Fabrication and Optical Test

320 × 240 THz focal plane array with with 35 μm pitch pixels was fabricated. The 35 μm – pitch pixel, shown in Fig. 3, is composed of diaphragm (sensitive area), cell contact and two legs which support the diaphragm. The diaphragm consists of support layer, thermal sensitive layer, passivation layer and THz absorption layer, with a reflection layer placed 2.5 μm away. The signal of the diaphragm is transferred via the cell contact to readout integrated circuit (ROIC) located under the reflection layer.

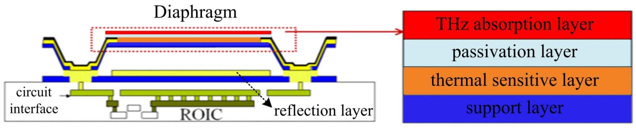

Fig. 3 Structure of single pixel in THz focal plane array

The reflection layer was made of NiCr thin film with a thickness of 250 nm which was also patterned as the bottom electrode by wet etching with a solution of ammonium cerium nitrate ($(NH_4)_2Ce(NO_3)_6$) and nitrate (HNO_3). To prepare suspended micro bridge, Photo sensitive polyimide pattern with a thickness of 2.5 μm was prepared as sacrificial layer on the reflection layer, which could be removed by oxygen (O_2) plasma. The diaphragm was fabricated on the sacrificial layer. 250 nm Si_3N_4 thin film acting as the support layer was deposited by plasma enhanced chemical vapor deposition (PECVD) from SiH_4/NH_3 at a temperature of 350 ℃, and patterned by RIE using a gas mixture of CHF_3 and O_2. VO_x thin film was prepared on the support layer as the thermal sensitive layer with a film thickness of 50 nm and a temperature coefficient of resistance (TCR) of ~ -2.3 %/K by magnetron sputtering with a sputter power of 300W, a partial pressure of oxygen of 0.5 %, and an annealing temperature of 350°C at vacuum environment. A Si_3N_4 passivation film was deposited on VO_x layer by PECVD with a thickness of 100 nm, on which Ti thin film acting as THz wave absorption layer was fabricated. Here, 20 nm Ti thin film directly deposited by magnetron sputtering and 9 nm Ti thin film thinned by RIE were prepared and patterned, respectively. 320 × 240 THz focal – plane array without Ti thin film absorber was also fabricated. After etching the top membrane by RIE, the photo sensitive polyimide (sacrificial layer) was released completely by O_2 plasma at 280 °C to form suspended micro – bridge structure in each pixel. SEM image of single pixel and three-dimensional microscopic image of THz focal – plane array are shown in Fig. 4.

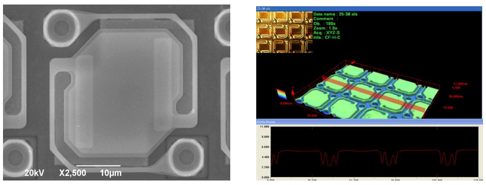

(a) (b)

Fig. 4 (a) SEM images of single pixel and (b) three – dimensional microscopic image of THz focal – plane array

The reflections of the fabricated 320 × 240 THz focal – plane arrays measured by the FTIR system are shown in Fig. 5. The reflections of THz focal – plane arrays with Ti absorption films are reduced compared to that of THz focal – plane array without Ti thin film absorber. 9 nm RIE treated Ti thin film shows greater contribution on the reduction of reflection. Since the transmission at the reflection layer in each pixel can be negligible and Ti absorption film is patterned on the top of the reflection layer, so the transmissions can be considered as a constant value for the three kinds of THz focal – plane arrays. Based on this assumption, it can be concluded that lower reflection of THz focal – plane array is caused by its higher THz absorption. It is clear that 9 nm RIE treated Ti thin film provides higher absorption of THz radiation. This provides an effective way which is easy to accomplish and compatible with the manufacturing process of THz focal – plane array to fabricate THz absorption layer and improve detection performance.

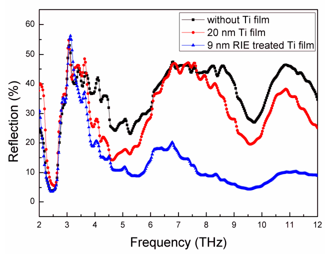

Fig. 5 Measured reflections of 320 × 240 THz focal-plane arrays without Ti absorption film and with Ti absorption film

Readout Circuit and Vacuum Packaging

Readout integrated circuit (ROIC) of 320 × 240 THz focal-plane array, fabricated in the substrate under the focal array, is a highly integrated circuit which completes various functions of the terahertz detector in a single semiconductor chip. Its basic function is to convert and amplify the detected signal, and transmit the output signal to the imaging circuit. The change of the current signal of each pixel is read by integral amplification, sample hold and buffer output in voltage bias mode. The resistance change which shows different amount of absorbed radiation is obtained by current change and THz imaging is realized.

Fig. 6 shows an architecture of ROIC for THz focal-plane array, which is composed of unit circuit (input stage), column signal processing circuit, high speed buffer output stage, line /column selection signal generating circuit and clock control signal generating circuit.

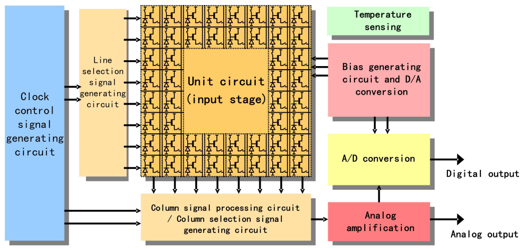

Fig. 6 Architecture of ROIC for THz focal – plane array

When a constant voltage is applied to the pixel, a large current value is generated (called the background current signal) due to high resistance value even without target radiation. If this current is amplified by integral, the integrator output is very easy to reach saturation and unable to characterize the amount of radiation. Due to the existence of non uniformity, dynamic range of output will be lost and the imaging quality will be seriously affected. So the elimination of high background signal and non uniformity is particularly important.

The elimination of high background signal is achieved by chosing the useful signal current for integral amplification, which means the bias current change caused by the change of the resistance when the change of THz radiation is detected by the pixel. The schematic diagram of circuit for background signal elimination is shown in Fig. 7 (a), in which I_3, rather than I_2, is integral amplified. The non uniformity is eliminated by correlated double sampling shown in Fig. 7 (b). Non uniformity caused by the offset of operational amplifier is eliminated using this circuit.

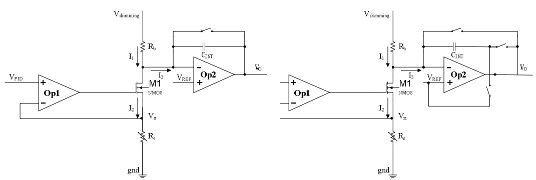

(a) (b)

Fig. 7 schematic diagrams of (a) circuit for background signal elimination and (b) correlated double sampling circuit

As shown in Fig. 7, the resistance of the pixel (R_s) has a very small change since a small change of the amount of radiation is detected. So I_3 is a very weak signal which is pA magnitude. In addition to amplifying useful weak signal, the ROIC should also suppress or reduce noise for higher signal to noise ratio (SNR) of output signal. Weak signal can be read out by appropriately increasing integral time and reducing integral capacitance. High frequency noise can be reducd by the frequency response characteristic of low – pass filter in the integrator. Low frequency noise can be eliminated by the method of correlated double sampling. The coupling noise of the substrate is eliminated by trap isolation for the integral capacitance and the sample – hold capacitance. The output dynamic range of the ROIC achieved 0.4V~3.6V and the fixed pattern noise (FPN) noise was less than 10 mV.

In order to improve the response, the detector was vacuum packaged to reduce the thermal conductivity, heat radiation and noise. Vacuum packaging structure for THz detector is mainly composed of shell (socket), thermoelectric cooler (TEC), ceramic substrate, detector chip, getter, thermal baffle, cap and optical window. All components are assembled into a complete vacuum packaged system by high precision assembly, as shown in Fig. 8.

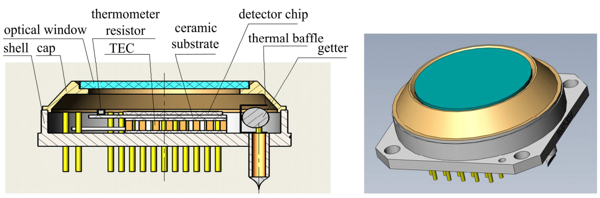

(a) (b)

Fig. 8 Structure diagram (a) and appearance diagram (b) of vacuum packaging structure

TEC was used to provide a stable operating point to the chip. Getter was integrated to adsorb the gas generated inside the assembly for a stable high vacuum. Due to relatively high temperature for the activation of getter, a thermal baffle was designed to keep thermal radiation of getter from detector chip and TEC and prevent damages during the activation process. TEC was welded to shell by metal welding for heat radiation and reliable connection. Optical window was welded to the cap by eutectic furnace welding and the cap is then welded to the shell with all other components fitted inside by laser welding to form a packaged assembly. After exhaust and pinch sealing, vacuum in the shell was higher than 10^{-5} Pa and leakage rate of the packaged assembly was measured to be lower than 2×10^{-13} Pa.m^3/s.

Terahertz Detection and Imaging

Firstly, Responsivity and *NEP* of single pixel vacuum packaged in a dewar bottle were mearsured by response and noise tests. Responsivity (*R*) of the sensing element can be calculated with the expression: $R = V_{out}/F$, where V_{out} is the value of response voltage and *F* is the incident power radiated to the sensing element. With the value of *R* and noise voltage (V_n), *NEP* can be calculated with the expression: $NEP = V_n/R$.

The tests were carried out with an environment temperature of 296 K and a relative humidity of 50%. The dewar with THz detector inside was connected to pump which kept the vacuum level inside the dewar under 1×10^{-3} Pa. A constant current offset of 1 μA was applied to the sensing element by a low noise current source (KEITHLEY 4200). When doing noise voltage test, small signal noise voltage was measured by a phase – locked amplifier (SR850) without target radiation. For response voltage test, a high power CO_2 laser (FIRL 100) which generated 2.52 THz radiation was used as THz radiation source. Because of the poor uniformity of the beam with a beam width of 10 mm and a divergence angle of 13 mrad, a throughhole with a diameter of 5 mm was set in the center of the beam in the light path. The radiation power through the throughhole and an optical window was measured to be 5.7 mW at the detector position by a THz power meter (Vector H410). The THz radiation power on single sensing element (35 μm × 35 μm) was calculated to be 0.3558 μW (under the assumption that the laser power was equal in the whole throughhole area which was much smaller than the beam). By setting the reference frequency and chopping frequency to 20 Hz, the noise voltage and peak value of response voltage of the sensing element were tested to be 100 nV/Hz$^{1/2}$ and 1.1 mV, respectively. So the responsivity was calculated to be 2186 V/W and the *NEP* was measured to be 45.7 pW/Hz$^{1/2}$.

The experimental arrangement for THz imaging is shown in Fig. 9. THz beam generated by CO_2 laser was collected and focused with two off-axis paraboloid mirrors onto the THz focal plane array through the silicon optical window on the vacuum packaged assembly. As shown in Fig. 10, images of a metallic circular washer covered by a piece of wiping cloth and a paper clip hidden in an envelope were obtained by the detector. Fig. 10(c) shows a THz image of the metallic circular washer covered by a piece of wiping cloth (made from 100 % polyester fiber), demonstrating the feasibility of security checking. Fig. 10(f) shows a THz image of the paper clip hidden in an envelope (made from kraft paper), demonstrating the feasibility of mail screening.

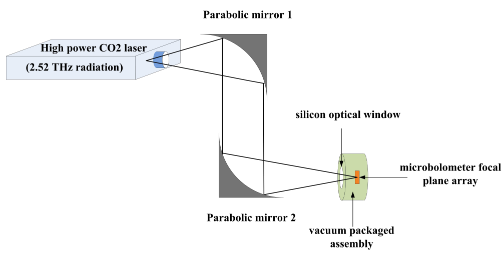

Fig. 9 Experimental setup for THz imaging (solid lines: paths of THz beams)

In conclusion, our imaging system demonstrates the use of a 320 × 240 THz focal plane array for real-time, continuous-wave 2.52 THz imaging with a far infrared CO_2 laser. Improvements in spatial resolution can be made by designing pixel structure and optics including using different radiation absorbing materials and fabricating appropriate antireflective structures on the optical window.

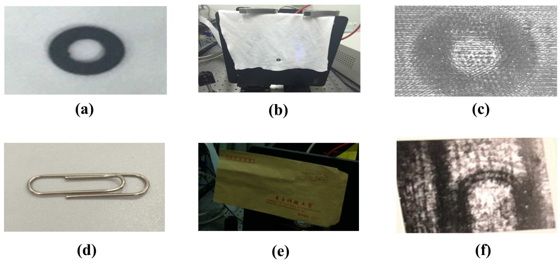

Fig. 10 White-light and THz images of covered metallic circular washer and hidden paper clip: (a) white-light image of metallic circular washer; (b) white-light image of metallic circular washer covered by a piece of wiping cloth; (c) THz image of the covered metallic circular washer; (d) white-light image of paper clip; (e) white-light image of paper clip hidden in an envelope; (f) THz image of the hidden paper clip

Conclusions

320 × 240 VO_x THz focal plane array was fabricated for THz detection and imaging coupled with a 2.52 THz CO_2 laser acting as THz illumination source. A nanostructured Ti thin film absorber prepared by a combined process of magnetron sputtering and RIE was integrated in the micro – bridge structure for improved THz absorption. By designing proper circuits including correlated double sampling circuit, the elimination of high background signal and non uniformity were achieved. Higher SNR was obtained by amplifying useful weak signal and reducing noise. The fabricated THz focal plane array was vacuum packaged in an assembly with a vacuum level higher than 10^{-5} Pa and a leakage rate lower than 2×10^{-13} Pa.m^3/s. Responsivity and *NEP* of the fabricated sensing element were measured to be 2186 V/W and 45.7 pW/Hz$^{1/2}$, respectively. THz images of a metallic circular washer covered by a piece of wiping cloth and a paper clip hidden in an envelope were obtained by the detecting system, demonstrating the feasibility of security checking and mail screening.

Acknowledgements

This work was supported by National Science Funds for Creative Research Groups of China (No. 61421002), the National Natural Science Foundation of China (Grant Nos. 61501092, 61235006, 61405027).

References

1 J. F. Federici, B. Schulkin, F. Huang, D. Gary, R. Barat, F. Oliveira and D. Zimdars, Semiconductor Science and Technology, 2005, **20**, S266-S280.
2 K. Kawase, Optics & Photonics News, 2004, **15**, 34-39.
3 S. M. Kim, F. Hatami, J. S. Harris, A. W. Kurian, J. Ford, D. King, G. Scalari, M. Giovannini, N. Hoyler, J. Faist and G. Harris, Applied Physics Letters, 2006, **88**, 153903.
4 Z. D. Taylor, R. S. Singh, M. O. Culjat, J. Y. Suen, W. S. Grundfest, H. Lee and E. R. Brown, Optics Letters, 2008, **33**, 1258-1260.
5 A. W. M. Lee, S. Kumar, B. S. Williams, Q. Hu and J. L. Reno, "Real-Time Imaging Using a 4.3-THz Quantum Cascade Laser and a 240×320 Element Focal-Plane Array," session CMLL2, CLEO/QELS 2006, Long Beach, CA, May (2006).
6 P. Kruse, R. Dodson, S. Anderson, L. Kantor, M. Knipfer, T. McManus, A. Wood and T. Rezachek , Proceedings of SPIE, 1998, **3436**: 572–577.
7 D. F. Murphy, M. Ray, R. Wyles, J. F. Asbrock, N. A. Lum, J. Wyles, C. Hewitt, A. Kennedy, D. Van Lue, J. S. Anderson, D. Bradley, R. Chin and T. Kostrzewa, Proceedings of SPIE, 2003, **4820**: 208–219.
8 B. S. Backer, N. R. Butler, M. Kohin, M. N. Gurnee, J. T. Whitwam and T. Breen, Proceedings of SPIE, 2002, **4721**: 83–90
9 C. Li, G. D. Skidmore, C. Howard, C. J. Han, L. Wood, D. Peysha, E. Williams, C. Trujillo, J. Emmett, G. Robas, Jardine, C-F. Wan and E. Clarke, Proceedings of SPIE, 2007, **6542**: 65421Y.
10 A. W. M. Lee, B. S. Williams, Q. Hu and J. L. Reno, IEEE Photonics Technology Letters, 2006, **18**: 1415–1417.
11 B. N. Behnken, M. Lowe, G. Karunasiri, D. Chamberlain, P. Robrish and J. Faist, Proceedings of SPIE, 2007, **6549**: 65490C.
12 A. W. M. Lee and Q. Hu, Optics Letters, 2005, **30**: 2563–2565.
13 B. N. Behnken, G. Karunasiri, D. R. Chamberlin, P. R. Robrish and J. Faist, Optics Letters, 2008, **33**: 440–442.
14 H. Budzier and G. Gerlach, Thermal infrared sensors: Theory, Optimization and Practice, Wiley, West Sussex, 226 (2011).
15 M. J. Coppinger, N. A. Sustersic, J. Kolodzey and T. H. Allik Optical Engineering, 2011, **50**: 053206.
16 A. Thoman, A. Kern, H. Helm and M. Walther, Physical Review B, 2008, **77**: 195405.
17 F. Alves, A. Karamitros, D. Grbovic, B. Kearney and G. Karunasiri, Optical Engineering, 2012, 51: 063801.
18 J. Gou, Y. Jiang and J. Wang, Micro & Nano Letters, 2014, **9**: 215–217.
19 J. Gou, J. Wang, W. Li, H. Tai, D. Gu and Y. Jiang, Journal of Infrared, Millimeter and Terahertz Waves, 2013, **34**: 431–436.
20 C. Bolakis, D. Grbovic, N.V. Lavrik and G. Karunasiri, Optical Express, 2010, 18: 14488–14495.
21 J. Gou, J. Wang, W. Li, D. Gu and Y. Jiang, Journal of Infrared, Millimeter and Terahertz Waves, 2015, **36**: 838–844.
22 A. Y. Vorobyev, A. N. Topkov, O. V. Gurin, V. A. Svich and C. L. Guo, Applied Physics Letters, 2009, **95**: 121106.